PREPRINT UCRL-79345

CONF-770938--1

Lawrence Livermore Laboratory

HYDRODYNAMIC MODELING AND EXPLOSIVE COMPACTION OF CERAMICS

C. Hoenig
A. Holt
M. Finger
W. Kuhl

September 1, 1977

This paper was prepared for presentation at the 6th International Conference on High Energy Rate Fabrication, September 9-16, 1977, Essen, Germany, and will be published in the proceedings.

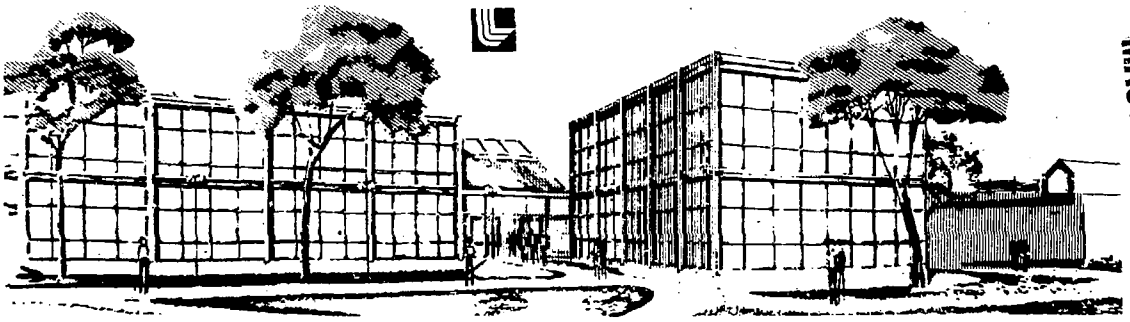

HYDRODYNAMIC MODELING AND EXPLOSIVE COMPACTION OF CERAMICS*

Lawrence Livermore Laboratory, University of California
Livermore, California 94500

Abstract

High-density ceramics with high-strength microstructure have been achieved by explosive compaction. Well characterized Al_2O_3, AlN, and boron powders were explosively compacted in both cylindrical and flat plate geometries. In cylindrical geometries we achieved compacted densities between 91 and 98% of theoretical. Microhardness measurements indicated that the strength and integrity of the microstructure was comparable to conventionally fabricated ceramics even though all samples with densities >90% theoretical contained macrocracks. Fractured surfaces evaluated by SEM showed evidence of boundary melting.

Equation of state data for porous Al_2O_3 were used to calculate the irreversible work done on the sample as a function of pressure. This was expressed as a percentage of the total sample which could be melted. Calculations show that very little melting can be expected in samples shocked to less than 3 GPa. Significant melting and grain boundary fusion can be expected in samples shocked to pressures >8 GPa.

Hydrodynamic modeling of right cylinder compaction with detonation at one end was attempted using a two-dimensional computer code. The complications of this analysis led to experiments using plane shock waves. Flat plate compaction assemblies were designed and analyzed by 2-D hydrodynamic codes. The use of porous shock attenuators was evaluated. Experiments were performed on aluminum oxide powders in plane wave geometry. Microstructure evaluations were made as a function of location in the flat plate samples.

Introduction

There has been a long-standing interest in using explosives to compact ceramic metal powders.[1-8] Even though ceramics powders have been compacted to relatively high bulk densities (>95% theoretical) it has been difficult to produce crack-free material. The cracking is generally associated with high rates of pressure release from shock-wave rarefaction. Since this results in tensile or shear forces that can exceed the strength of ceramic materials, metal containers are necessary for reinforcement.

Several investigations[1,2,7,9] have explored the problem of converging shock wave compaction in a cylindrical geometry. Bogdanov, et al.[10] reviewed earlier attempts to develop a mathematical model for powder compaction. They also presented their own analysis for metal powders and flat high-explosive charges assuming that the powders behave as an ideal compressible liquid. Experimentally, they compacted titanium powder onto both hard and soft base supports. They observed good correlation between experiment and theory regarding density variations in flat compacted powder samples up to 50 cm in thickness.

* Work performed under the auspices of the U.S. Energy Research & Development Administration under contract No. W-7405-Eng-48.

Our work was motivated by the need to develop fabrication methods for ceramics and composite materials that are difficult, costly, and sometimes impossible to fabricate by more conventional methods. We selected three ceramic materials (Al_2O_3, AlN, and boron) for our initial study, emphasizing Al_2O_3 for two reasons. First, Al_2O_3 is one of the major raw materials used in the ceramic industry. Second, aluminum oxides of varying ourity, crystallinity and porosity have been the object of several shock wave and explosive compaction investigations.[11-14] The information from these studies together with other well-known physical properties provided background information for our modeling studies.

Experimental

Starting Materials

Alpha alumina (Alcoa Tabular, Grade T-61*) powder was used in all experiments with Al_2O_3. The powder had been converted to the alpha phase by treating it at a temperature slightly below melting (<2040°C) and grinding it to pass a 100-mesh screen. The as-received particle size range was 10 to 177 μm. Particles contained some closed porosity, and particle densities measured by mercury porosimetry were in the range of 3.81 to 3.91 g/cm^3 (theoretical = 3.97 g/cm^3). A powder surface area of 0.3 m^2/g was measured by the N_2 absorption BET method.

Aluminum nitride powders were used as received with a particle size range of 10 to 300 μm. Particle densities were in the range of 3.18 to 3.26 g/cm^3 (theoretical = 3.26 g/cm^3).

Crystalline boron powder was supplied by Herman C. Stark, Berlin with a particle size range of 44 to 105 μm. Particle densities were >2.32 g/cm^3 (theoretical = 2.34 g/cm^3).

The initial bulk density of powder before compaction was ~65% for Al_2O_3 and ~55% for AlN and boron.

Compaction Assemblies

Both cylindrical and flat-plate-geometry high explosive compaction assemblies were used in this study. The cylindrical assembly was very similar to those used by Prümmer[1] and Staver[2] in their earlier investigations. It consisted of mild steel tubes (2.54-cm o.d./0.165-cm wall and 1.27-cm o.d/0.165-cm wall, lengths ≈18 cm) loaded with sample powders and mounted concentrically inside a plastic container which held the high explosive. The tubes were not evacuated. A conical wave guide also functioned as a plug at the top. Detonations occur at one end. Timing pins were located along the plastic tube to check the detonation velocity of the explosive. This assembly was suspended 1 m above the ground by means of a wooden frame. After compaction, the remarkably straight tubes were imbedded in the soil approximately 30 cm. The surface temperature rises of the order of 600 to 800K. Samples of Al_2O_3 required

*Reference to a company or product does not imply approval or recommendation of the product by the University of California or ERDA to the exclusion of others that may be suitable.

annealing in air at 1375 K for ~36h in order to remove them intact from the metal container. Both AlN and boron could be removed without prior annealing.

The flat plate assembly is shown in Fig. 1. All experiments using this assembly were done with Al_2O_3. Powders were loaded into an all aluminum sample holder which fit loosely into the outside aluminum tube. The size of the sample chamber was 5.08 cm dia. × 0.95 cm. ht. The lid was welded in place. Stepped transducer pins were located at the center and edge positions to evaluate shock-wave velocity and planarity. Layers of aluminum powder of decreasing density were placed just beneath the sample holder in an attempt to attenuate shock wave reflections from the surface at the bottom of the sample holder. High explosive was loaded above and in direct contact with the sample holder. A timing pin activated the scopes for the transducer pins mentioned previously. A plane wave detonation lens assembly was in direct contact with the high explosive.

Three samples of aluminum oxide were compacted using this assembly. In shot KB 001 a fully dense, sintered Al_2O_3 sample (Coors AD 995) was compacted as a control. In shots KB 002 and KB 003, as-received Tabular Al_2O_3 powder was loaded to bulk densities 62% of theoretical. Flake TNT at a density of 0.95 g/cm^3 and a detonation velocity of 4.9 km/s yielded a detonation pressure of 6.0 GPa. The detonation pressure was calculated according to the expression:

$$P = \frac{\rho D^2}{\gamma + 1} ,$$

where P is the pressure in GPa, D is the measured detonation velocity (km/s), ρ is the density of the explosive, and γ is the polytropic gas parameter of the detonation products $(d \ln P/d \ln V)_S$ and is usually taken as being equal to 2.75 for ideal explosives such as PETN and TNT.[15] The calculated detonation pressure is in good agreement with P measured for TNT[16] and PETN.[17] The heights and weights of explosive used were 5.72 cm, 0.583 kg for shots KB 001 and KB 002, and 22.86 cm, 2.331 kg for shot KB 003. The entire assembly was partially immersed in a barrel of water to the approximate level of the plane wave lens.

After compaction the sample holders were retrieved and radiographed for density variations and crack patterns before disassembly. Finally the alumina samples were removed and specimens were taken along a radial location for microstructural analysis.

Discussion of Results

In our experiments with Al_2O_3 in cylindrical geometry we found that the initial powder density was an important factor in achieving final compacted densities >90% theoretical. This factor was not as important for AlN and boron. The results of cylindrical compaction are listed in Table I.

Compacted densities between 94 and 98% of theoretical were achieved for Al_2O_3, AlN, and boron. As samples approached and exceeded 90% theoretical density macrocracking was observed in almost every case. As a check on bulk density and density uniformity, one Al_2O_3 sample compacted at 3.6 GPa (5.7 e/m*) was broken into three segments for mercury porosimetry evaluation.

Selected segments were representative of locations along the radius of the cylinder. The three porosity measurements were 8.18%, 8.74% and 7.95% indicating good compaction uniformity. These measurements also corroborate the measured overall bulk density of 92% theoretical for this sample.

Typical examples of compacted materials after removal of metal cladding are shown in Fig. 2. The samples were ground to final shape. The two Al_2O_3 samples were annealed in air at 1100°C for 36 h. The spiral cracking in Al_2O_3 is typical of the cracking behavior observed in Al_2O_3 samples with densities >91% of theoretical. The section without cracks has a density of 90% of theoretical. This is the highest Al_2O_3 density we were able to get without cracking. The crack profiles in Al_2O_3 indicate that the samples failed in shear during the decompression phase of the compaction process.

The compaction and cracking behavior of AlN and boron were unlike that of Al_2O_3. Higher densities (97-98% theoretical) were achieved under nearly equivalent compaction conditions. Extensive shear fractures like those observed in Al_2O_3 were absent. The crack patterns shown in Fig. 2 appear to be associated with an axial melt region and possible differences in thermal expansion. The boron sample, in particular, has a central core that appears to have melted. The microstructure and microhardness of this region were different than the outer regions. Both regions in the boron have equivalent densities (~97% theoretical) as determined by separate mercury porosimetry measurements. The overall structural integrity of both AlN and boron samples was significantly better than that of Al_2O_3.

Even though most of the Al_2O_3 samples in this series experienced some macrocracking, the bulk material after compaction appeared to have a quality comparable to materials which are sintered or hot pressed. Therefore, representative samples were prepared for microhardness and microstructural evaluations (Fig. 3). A sample compacted at 7.7 GPa (e/m = 3.8) contained a small central core in which melting appears to have occurred. All signs of the characteristic particle porosity, which is still evident in the middle to edge view, have vanished. Grains also appear rounded and cusp-shaped indicating melting. Also in Fig. 3 we show a polished surface after ion-etching. We believe that polishing has damaged and cracked the microstructure resulting in "pullouts" and artifical fractions. The ion-etched surface is more indicative of the actual mircostructure of a compacted sample. This surface continues to show particle porosity but indicates essentially crack-free material compared to the as-polished section.

Microhardness

Average Knoop microhardness values for explosively compacted samples are listed in Table I. The two Al_2O_3 samples are listed in the order of increasing detonation pressure and e/m ratio. Measurements were taken at the center and along the radius with 100 and 500 g loads. Average values were determined from 3 to 6 measurements and errors were reported as the standard

---

★ Mass ratio of explosive to ceramic powder.

deviation (±). For comparison, literature values (HK^{100}) and our own value for hot-pressed Tabular Al_2O_3 (HK_{500}) are as follows:

Al_2O_3 (Sapphire, c-axis)[18]		2000 ± 100 kg/mm^2
(Hot pressed, 1810°C, 95% Theo. Den.)		1580 ± 190 kg/mm^2
AlN, Single Crystal[19]	($\perp$ c-axis)	1440 ± 60 kg/mm^2
	($\parallel$ c-axis)	1020 ± 60 kg/mm^2
Boron,		2760 ± 200 kg/mm^2 (HV_{100}, Vickers)[20]
		3400 kg/mm (HV_{50}, Vickers)[21-22]

Hardness values are inversely dependent on load and are most often reported using a 100-g load. We have extended the range of loads to 500 g in order to better assess the strength of compacted microstructures.

At 100-g loads for Al_2O_3, there is no statistical difference in the hardness of samples compacted at 3.6 and 7.7 GPa. Hardness values at this loading also compare favorably with values reported in the literature. At 500-g loads, however, the data indicates that Al_2O_3 compacted at 3.6 GPa is much softer than that compacted at 7.7 GPa – regardless of location along the radius.

The hardness for AlN at 100-g loads varied significantly from center to edge. Values of 2050 ± 80 kg/mm^2 (center) and 1600 ± 200 kg/mm^2 (edge) are both greater than those reported in the literature[19] for small single crystals. At 500-g loads, there was no difference between center and edge locations.

The hardness measurements for boron in the central core region yielded values only slightly greater than those reported in the literature.[20-22] The values for the central core HK_{50} = 4000 ± 260 kg/mm^2 and HK_{100} = 3170 ± 120 KG/mm^2 were ~15% higher than those reported elsewhere. Measurements at both 100-and 500-g loads clearly indicate a difference between the central core and outer regions. In spite of equivalent bulk densities, the central core is approximately 50% harder than material outside the core. These central-core indentations have been measured with an oil immersion lens. Even at these high magnifications, however, endpoint determinations for such small indentations are difficult to measure.

The AlN and boron samples were not annealed. An x-ray analysis of both the AlN and boron samples indicated normal patterns with no significant residual stresses. We did find significant residual stresses in the compacted Al_2O_3 samples. Stresses and dislocation densities were determined by calculation to be in the order of those reported by Prümmer.[13] Prümmer measured lattice distortions up to 0.35% and dislocation densities up to 10^{11} cm^{-2} in explosively compacted Al_2O_3.

Scanning Electron Microscopy

Three samples were selected for scanning electron microscope (SEM) evaluations. Samples were first cut into discs and then loaded in dimetral compression[23] to produce tensile failure along the diameter. As expected, failure also occurred

in some cases along the "spiral-like" shear cracks shown in Fig. 2, which were the result of explosive compaction. In our discussion, we will refer to these surfaces as spiral and the other surfaces as tensile. A spiral surface for Al_2O_3 compacted at 3.6 GPa is shown in Fig. 4. A tensile fracture surface for Al_2O_3 compacted at 7.7 GPa is shown in Fig. 5.

The spiral crack surfaces of Al_2O_3 compacted at both 3.6 and 7.7 GPa were essentially equivalent. The low magnification view in Fig. 4 shows a wave-like sinusoidal topography with an unusually smooth surface texture. At higher magnifications, very fine-grained regions (~0.1 μm) show evidence of incipient melting. It is difficult to tell how deep this fine-grain material penetrates into the bulk sample, but it appears to be very superficial.

The tensile surface at low magnification (Fig. 5) shows a combination of inter- and intragranular fracture. Views at higher magnification show the nature of the fine-grain material, which interfaces and bonds together the larger grains. The views at 500X and 2500X magnification for Al_2O_3 compacted at 7.7 GPa show the development of a smooth-fused and dense layer of material between grains. We believe the intrinsic strength of this microstructure should be greater than that for Al_2O_3 compacted at 3.6 GPa. This analysis is supported by the microhardness values at 500-g loads listed in Table I.

The tensile fracture surface for AlN compacted at 7.4 GPa is shown in Fig. 6. As with Al_2O_3, the mechanism appears to be a combination of inter-and intragranular fracture. The higher magnification views at 2500X and 10 000X also indicate that this material is very fine grained (<1 μm) and that all grains are very well fused together. This explains in part why the sample shown in Fig. 2 was capable of being polished to a very fine surface finish. It also supports the relatively high strength of AlN as compared to Al_2O_3.

Plane Wave Compaction

Only a few exploratory tests have been made using the plane wave compaction assembly described earlier (Fig. 1). Tests were conducted at 6.0 GP detonation pressure using flake TNT. A typical recovered sample chamber partially disassembled is shown in Fig. 7. Radiographs were taken before disassembly.

The fully dense Al_2O_3 sample (KB 001) was cracked as expected. The approximate pattern of cracking indicated that unloading in the radial direction produced a circular crack about 4 cm in parameter near the outer circumference of the disc. There were also radial cracks with origins at the center of the disc. We believe these cracks are the result of a nonplanar shock wave, which exerted a maximum pressure at the center of the disc. Similar crack patterns have been noted in biaxial flexure tests of ceramic discs[24] in which the area of maximum tensile stress occurs at the center of the lower face. The lack of planarity may have been the result of inhomogeneities in the flake TNT explosive. On the other hand, we also believe that the thickness/diameter ratio of explosive should be increased.

The two plane wave tests involving the compaction of Tabular Al_2O_3 (10-177 μm) also used flake TNT at a detonation pressure of 6.0 GPa. They differed only in the height of explosive. Shot KB 002 used an HE height of 5.72 cm similar to the shot with fully dense Al_2O_3. Shot KB 003 shown in Fig. 7 used an HE height of 22.96 - four times that used for KB 002.

Both tests (KB 002 and KB 003) did not achieve the high density Al_2O_3 compaction that was obtained in the cylindrical compaction previously discussed. The compacted powders did exhibit significant strength and coherence, however, even though the densities were estimated to be only 85 to 90% of theoretical. Photomicrographs of the microstructure at center and edge locations are shown in Fig. 8. Both edge and center views are shown at low magnification. It appears from Fig. 8 that the outer regions of the samples have fewer voids and were compacted to a slightly higher strength or density than the central locations.

Hydrodynamic Modeling

On the basis of our limited experimental observations, we can hypothesize a sequence of events during shock compaction that explain how ceramic powders bond together to provide bulk strength. We will confine our attention to hard brittle materials, which exhibit little plastic flow during the shock compaction process. We expect the materials used in this study — Al_2O_3, AlN, and boron — to behave in this manner.

Aluminum nitride may be an exception however, since recent triaxial compression studies by Cline and Heard[25] indicate that AlN exhibits a brittle-ductile transition at confining pressures as low as 0.5 GPa. Aluminum oxide exhibits brittle behavior at confining pressures up to 1.25 GPa, the upper limit of measurement in this study.[26] The ductile-brittle transition for Al_2O_3 was estimated to be in excess of 3 GPa. We believe these studies may have a significant bearing on the explosive compaction behavior of AlN and Al_2O_3 observed in this investigation. However, in view of the high strain rates employed in explosive compaction, even AlN probably behaves as a brittle material during consolidation.

As noted by Prümmer[6] most of the volume change that takes place during shock compaction is due to fracture and rearrangement of particles to minimize pore or void volume. We hypothesize that frictional forces across grain boundaries and fractured surfaces cause localized surface melting. The energy deposited by the shock wave is insufficient to raise the entire sample above the melting point. Subsequent thermal conduction toward the center of particles therefore causes the small melt regions to rapidly solidify. However, the temperature is sufficient to generate strong bonds between particles. The existence of these transient high temperatures at contact surfaces is the important difference between shock wave compaction and low-strain-rate isothermal compaction.

To test this hypothesis, we estimated the amount of energy available for melting, as a function of shock pressure for Al_2O_3 powder at an initial 65% theoretical density. For our calculations, we used the pressure-volume relation of Seaman, Tokheim, and Curran.[19] Although their data is for porous Al_2O_3, we believe it can reasonably be applied to a powder since the porous materials are easily broken up during the initial phase of shock compression. With this data we can calculate the amount of available irreversible energy as a function of shock pressure in order to see its significance relative to melting some fraction of the sample. The result is shown in Fig. 9. Here we plot the ratio of E_{irrev} to the energy necessary to melt the sample. For the

purpose of this calculation we use 109 kJ/mol (26 kcal/mol) for the heat of fusion, 125 J/mol·deg (0.03 kcal/mol·deg for the specific heat, and 2030°C for the melting temperature. This energy is available for all irreversible physical processes (fracture, defect formation, frictional heating) that take place during shock compaction. The energy for creating lattice defects in these materials is negligible. The energy for work of fracture in ceramic powders is also small in comparison to E_{irrev}. For example E_{irrev} at 8 GPa is ≈1.67 GH/m³ (400 cal/cm³) for Al_2O_3. Using 50 J/m² (5×10^4 ergs/cm²) for the work of fracture[24] and Al_2O_3 spheres 100 μm in diameter, we calculate the maximum energy necessary to fracture each particle one time to be ≈837 kJ/m3 (0.2 cal/cm³) or ≈0.05% of E_{irrev} for shock pressure at 8 GPa.

We would like to emphasize that the curve in Fig. 9 represents an upper bound for the fraction of the sample melted by the shock wave deposited because the energy will not be optimally distributed for melting the sample. For example, some energy will be deposited in portions of the sample that never reach the melt temperature. We also expect that for some materials such as AlN this type of calculation may not apply because a large amount of plastic flow may occur during particle compaction.

Our curve shows that very little Al_2O_3 melting can be expected in samples shocked to less than 3 GPa. It suggests that signficant melting and grain boundary fusion can be expected in recovered samples that have been shocked to about 8 GPa. Above 8 GPa the melt curve flattens out indicating that higher pressures may not be desirable. This is because the trade-off between additional available energy and the higher unloading stresses, which cause macrocracking, may be counter productive. These results are generally confirmed by the experimental studies presented earlier in the report.

Our experiments demonstrate that sound microstructures can be generated by explosive compaction. The major problem is to design an experimental geometry which can compensate for, or eliminate the unloading stresses which crack the sample. Numerical modeling of powder compaction experiments seem a logical next step to help solve this problem.

To this end, we have made some preliminary two-dimensional hydrodynamics calculations using the HEMP computer code. Unfortunately, HEMP does not contain an operational porous material model, so we had to approximate the behavior of the powder by means of a compressible fluid equation of state. This should give reasonable results for stress loading behavior, but will not be a good approximation for stress attenuation or unloading behavior.

Figure 10 shows a model calculation of explosive compaction of a cylindrical sample using an explosive that burns axially. This calculation has rotational symmetry about the vertical centerline of the dark central region. This region is the compressible fluid used to represent the Al_2O_3 powder sample. The thin region outside the sample represents the steel pipe jacket, which is represented in the calculation as an elastic, perfectly plastic material. Outside the jacket is the coarsely zoned high explosive, PETN. Because of the approximate nature of our powder equation of state, we have not attempted to obtain any quantitative information from this calculation. However, a study of the numerical results reveals the complicated nature of the stress-strain history experienced by the sample in this type of experiment. The main feature is a conical shock wave propagating toward the axis of the sample and

reflecting back toward the steel jacket. This wave reflects from the outer boundary of the jacketing material as a tensile wave, which would, in the absence of good strength in the jacketing material, cause the sample to come apart.

Although this is an easy geometry from which to recover a sample, we feel it has several important disadvantages. First, because the wave is converging it is difficult to know what shock pressure the sample experienced. Second, it has inherent size limitations. Third, it is difficult to instrument for making measurements. Lastly, we believe that beyond a certain pressure it may be impossible during the unloading phase to recover a sample without cracking it.

To overcome these problems, we have tried to design a new experiment, which subjects the sample to a single plane wave. The experimental configuration was described earlier in Fig. 1. A numerical calculation of this new geometry is shown in Fig. 11. This calculation has rotational symmetry about the left edge of the figure. The similarity between the predicted sample holder shape shown in Fig. 11 and the actual recovered shape shown in Fig. 7 is very encouraging. Again, we have only tried to draw qualitative conclusions about the experiment from the calculation. We were able to determine that in order for our sample to see a plane wave loading, both the sample and explosive will need to have a smaller thickness to diameter ratio than in our first experiments. The calculations also indicate that considerable improvement in the experiment can be realized by replacing the aluminum sample holder and tube with a stronger metal like steel, which will not fracture and flow as much.

Concluding Remarks

Our microhardness determinations and evaluations of microstructure have indicated that strong dense ceramic materials can be fabricated by explosive compaction in cylindrical geometry. The development of macrocracks during decompression remains a serious limitation in the utilization of explosives to fabricate ceramics. We believe, however, that these problems can be solved through experimental design and careful control of explosive parameters.

At the present time cylindrical geometries with axial symmetry offer the most promising shapes for successful compaction. It appears, however, that it may not be possible to scale up these geometries. This is certainly the case for solid cylinders. Scale up potentials for large tubes, and cones, appear to be much better if wall thicknesses are reasonable.

Plane wave compaction and the corresponding ease of computer modeling offers the most valuable tool in advancing the basic understanding of the compaction process. We also believe that the flat plate geometry offers considerable scale-up potential.

Many ceramics are essentially unavailable as engineering materials because they are difficult, if not impossible, to fabricate by conventional methods. For these materials and others, explosive compaction can become a useful and competitive fabrication technology in the future.

Acknowledgements

We gratefully acknowledge the important contributions made by several of our colleagues at Lawrence Livermore Laboratory. First and foremost we thank Mr. Jack Frazer, Mr. Jack Robbins, Mr. Harry Rizzo and the Chemistry and Materials Science Department for sponsoring this effort under our Chem Research Program. Mr. Ed Lee and Mr. John Walton gave valuable advice and assistance in setting up our modeling studies on the computer. Mr. Ron Boat helped organize and execute the high explosive experiments at Site 300. Metallographic preparations and analysis were provided by Mr. Al Ulrich. Particle Analysis and density measurements were provided by Mr. Charles Slettevold and Mr. Roy Lindahl. X-ray diffraction studies were done by Mr. Gordon Smith. Advice and counsel throughout the program were kindly given by Mr. Richard Landingham Mr. Carl Cline, Mr. Mark Wilkins, Mr. John Shaner, and Mr. Robert Schock.

Table I. Properties of Al_2O_3, AlN, and boron ceramics explosively compacted in cylindrical geometry.[a]

Material	Explosive parameters: Type	D, (km/s)	P (g/cm³)	Pressure, GPa	e/m ratio	Sample density, % theo.	Ave. microhardness (kg/mm²): HK_{50}	HK_{100}	HK_{500}
Al_2O_3[b] (10-177 μm)	PETN	4.2	0.70	3.6	5.7	92	NM[f]	2070 ± 240(C)[d]	710 ± 140(C) 770 ± 90(E)[e]
Al_2O_3[b] (10-177 μm)	PETN	5.5	0.95	7.7	3.8	91	NM	2280 ± 10(C)	1525 ± 170(C) 1200 ± 160(E)
AlN[c] (10-300 μm)	RDX	5.7	0.90	7.4	5.7	98	NM	2050 ± 80(C) 1600 ± 200(E)	1270 ± 100(C) 1200 ± 100(E)
Boron[c] (44-105 μm)	RDX	5.8	0.89	7.5	13.8	97	4000 ± 260(C)	3170 ± 120(C) 2200 ± 90(E)	2300 ± 60(C) 1340 ± 220(E)

[a] 2.54 cm od, 20 cm ht.

[b] Al_2O_3 samples annealed in air at 1100°C for 36 h.

[c] Not annealed.

[d] Measured at the center.

[e] Measured at the edge.

[f] NM = Not measured.

References

1. Prümmer, R., "Explosive Compaction of Ceramic and Metal Powders and Composites," Ber. Dt. Keram. Ges., 50, No. 3, p. 75-81 (1973).

2. Staver, A. M., "Physical Aspects of Explosive Compaction of Powders," (Inst. for Hydrodynamics. Novosibirsk, USSR) presented at 5th International Conference on High Energy Rate Fabrication, Univ. of Denver Research Inst., June 24-26, 1975.

3. Gorobtsov, V. G. and Roman, O. V., "Hot Explosive Pressing of Powders," Inter. Jour. of Powder Met. and Powder Tech., Vol. 11, No. 1, p. 55-60, (1975).

4. Leonard, R. W., "Direct Explosive Compaction of Powdered Materials," Battelle Tech. Rev. 17 (10) p. 13-17 (1968).

5. Bergmann, O. R. and Barrington, J., "Effect of Explosive Shock Waves on Ceramic Powders," Jour. Amer. Ceram. Soc., Vol. 49, No. 9, p. 502-507 (1966).

6. Carlson, R. J. Porembka, S. W., and Simons, C. C., "Explosive Compaction of Ceramic Materials," Bull. Amer. Ceramic Soc., Vol. 45, No. 3 (1966).

7. Deribas, A. A. and Staver, A. M., "The Shock Compression of Porous Cylindrical Bodies," Trans. from Fizika Goreniya i Vzryva, No. 4, p. 548-578 (1974).

8. Prümmer, R. A. and Ziegler, G., "Structure and Annealing Behavior of Explosively Compacted Alumina Powder," presented at 5th International Conference on High Energy Rate Fabrication, Denver, Colorado, June 24-26, (1975).

9. Kuz'min, G. E. and Staver, A. M., "Determination of the Flow Parameters With Shock Loading of Powdered Samples," Trans. from Fizika Goreniya i Vzryva, Vol. 9, No. 6, p. 898-905 (1973).

10. Bogdanov, A. P., Lazarev, A. S., Roman, O. V., and Furs, V. Ya., "Compression of Metal Powders by Flat High Explosive Charges," Part I, Trans. from Poroshkovaya Metallurgiya, No. 7 (127), p. 33-37 (1973) and Part II, Trans. from Ibid, No. 11 (131), p. 20-23 (1973).

11. Ahrens, T. J., Gust, W. H., and Royce, E. B., "Material Strength Effect in the Shock Compression of Alumina," Jour. of Applied Physics, Vol. 39, (No. 10), p. 4610-4616 (1968).

12. Gust, W. H. and Royce, E. B., "Dynamic Yield Strengths of C_4C, BeO and Al_2O_3 Ceramics," Ibid, Vol. 42, No. 1, p. 276-295, (1971).

13. Seaman, L., Tokheim, R. E., and Curran, D. R., "Computational Representation of Constitutive Relations For Porous Materials", Stanford Research Institute, DNA 3412f, May 1974.

14. Leiber, C. O., "Die Hugoiotelastische Grenze und die Dynamischen Druckfestigkeiten spro der Korper," Planseeberichte fur Pulvermetallurgie, Vol. 18, No. 3, p. 178-193, (1970).

15. Lee, E. L., Hornig, H. C., and Kury, J. W., "Adiabatic Expansion of High Explosive Detonation Products," Lawrence Livermore Laboratory Report, UCRL 50427, May 1968.

16. Finger, M., Lee, E., Helm, F. H., Hayes, B., Hornig, H., McGuire, R., Kahuia, M., and Guidry, M., "Effect of Elemental Composition on Detonation Behavior of Explosives," Sixth Symposium on Detonation, Aug. 1976.

17. Hornig, H. C., Lee, E. L., and Finger, M., "Equation of State of Detonation Products," Fifth Symposium on Detonation, Aug. 1970.

18. Palmour, Hayne III, Kriegal, W. W., and DuPlessis, J. J., "Microbrittleness Anisotropy in Thermally Etched Sapphire," Mech. Prop. of Eng. Ceramics, Ed. W. W. Kriegal and H. Palmour III, Interscience Publishers, 1961.

19. Taylor, K. M. and Louie, C., "Some Properties of Aluminum Nitride," Jour. Electrochemical Soc., Vol. 107, No. 4, p. 308-314 (1960).

20. Niihara, K and Hirai, T., "Chemical Vapor-deposited Silicon Nitride," Jour. of Materials Sci., Vol 12, p. 1243-1252 (1977).

21. Formstecher, M. and Ryschkewitsch, E., Compt. Rendu, vol. 221, p. 747 (1945).

22. Meerson, G. A. and Samsonov, G. V., Izv. Sektora Fiz. — Khim Analiza (News of the Dept. of Physiochemical Analysis) Vol. 22, p. 92 (1953).

23. Radnick, A., Hunter, A. R., and Holden, F. L., "An Analysis of the Diametral-Compression Test," Materials Research and Standards; April, p. 283-289, (1963).

24. Wachtman, J. B. Jr., Capps, W., and Mandel, J., "Biaxial Flexure Test at Ceramic Substrates," Jour. of Materials, JMLSA, Vol. 7, No. 2, p. 188-194 (1972).

25. Cline, C. F. and Heard, H. C., "The Mechanical Behavior of Polycrystalline BeO, Al_2O_3 and AlN at High Pressure," (to be published).

HLL/cak/acs/jjf

FIGURE CAPTIONS

Fig. 1. Flat-plate HE compaction assembly.

Fig. 2. Explosively compacted ceramics ground and polished after cleaning.

Fig. 3. Alumina after explosive completion at 7.7 GPa, e/m = 3.8. Air annealed at 1373 K, 36h. Note that the porosity is absent in the center view indicating that the center of the cyclindrical sample melted during explosive compaction. Also, the photograph of the sample that was ion thinned shows no cracks.

Fig. 4. SEM analysis of Al_2O_3 spiral surface compacted with PETN at 3.6 GPa and 5.7 e/m.

Fig. 5. SEM analysis of tensile surface of Al_2O_3 compacced to 91% theoretical density (PETN, 7.7 GPa, 3.8 e/m, vacuum annealed for 63 h at 1448 K.

Fig. 6. Tensile fracture surface of explosively compacted AlN (RDX, 7.4 GPa, 5.7 e/m, 98 theoretical density, not annealed.

Fig. 7. Edge view of a flate-plate Al_2O_3 compaction (TNT, 6.0 GPa). A piece of the aluminum container tube is shown at the left.

Fig. 8. Plane-wave compaction of Al_2O_3. (TNT, 6.0 GPa).

Fig. 9. Available irreversible energy expressed as percent of melt for porous Al_2O_3 as a function of shock pressure calculated from the Hugoniot of porous Al_2O_3 and the equation of state of solid Al_2O_3. Initial density = 65% of theoretical.

Fig. 10. Computer model of plane-wave compaction.

Fig. 11. Model calculation of cylindrical explosive compaction.

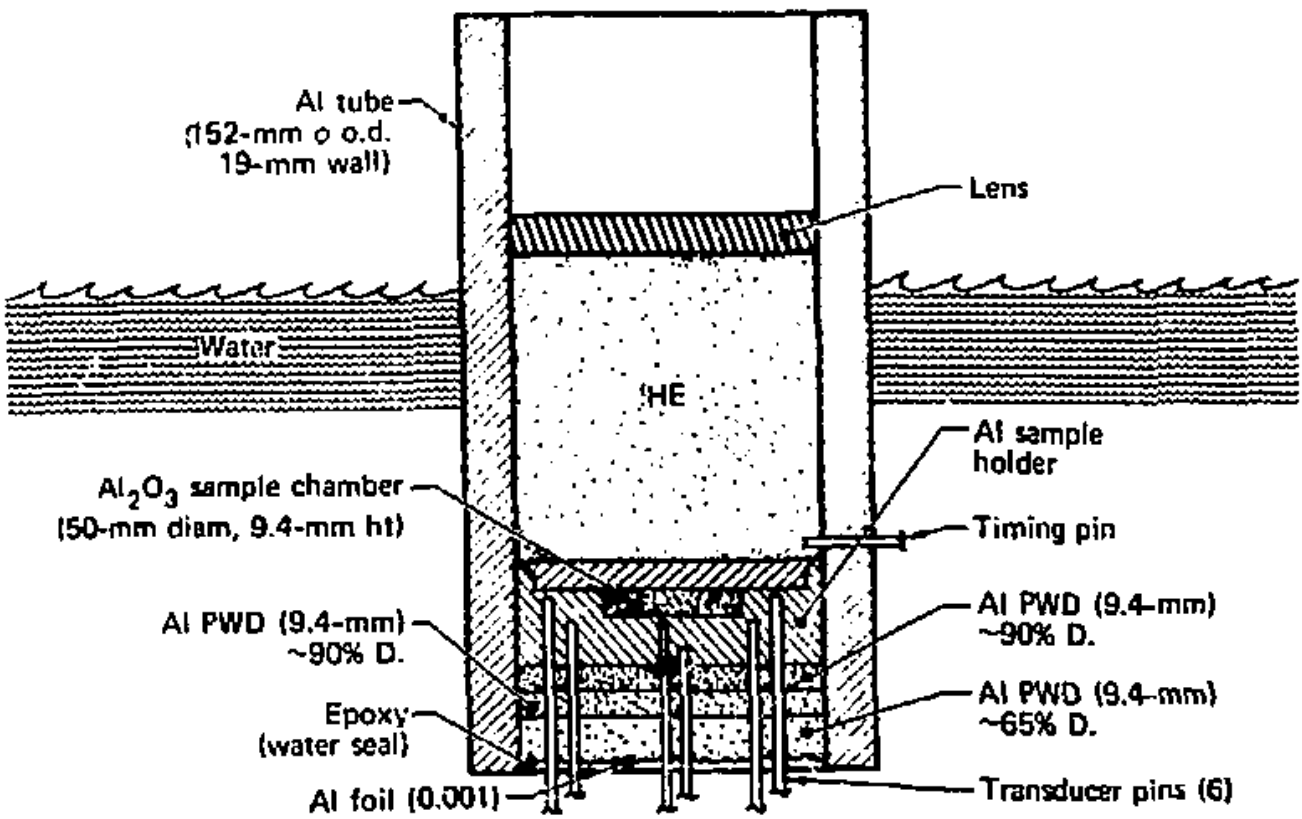
Al tube
(152-mm o o.d.
19-mm wall)
Lens
Water
HE
Al sample
holder
Al_2O_3 sample chamber
(50-mm diam, 9.4-mm ht)
Timing pin
Al PWD (9.4-mm)
~90% D.
Al PWD (9.4-mm)
~90% D.
Epoxy
(water seal)
Al PWD (9.4-mm)
~65% D.
Al foil (0.001)
Transducer pins (6)

Hoenig - Fig. 1

Boenig - Fig. 2

Edge of sample (after ion thinning)

Center of sample

Hoenig - Fig. 3

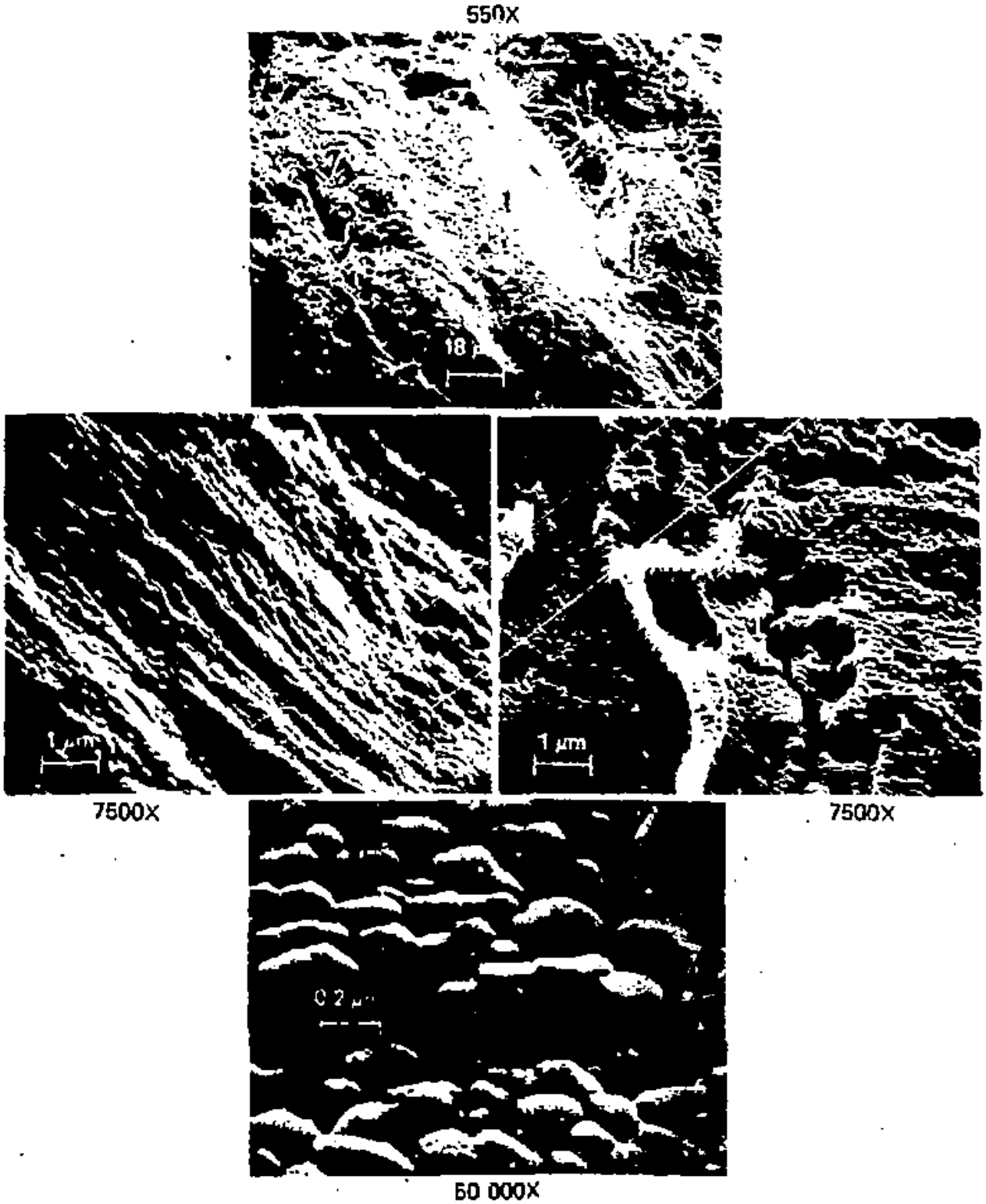

Roenig - Fig. 4

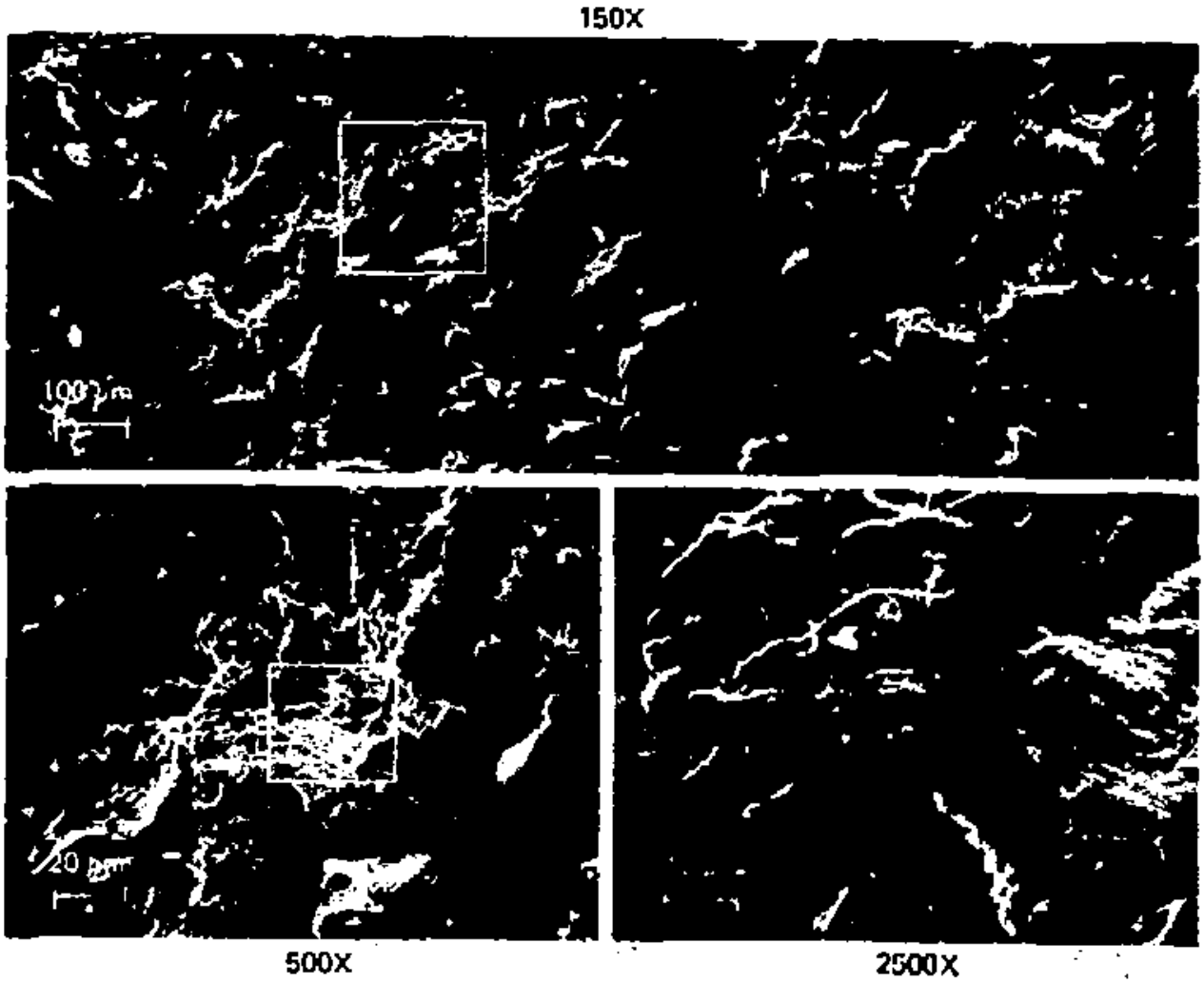

Hoenig – Fig. 5

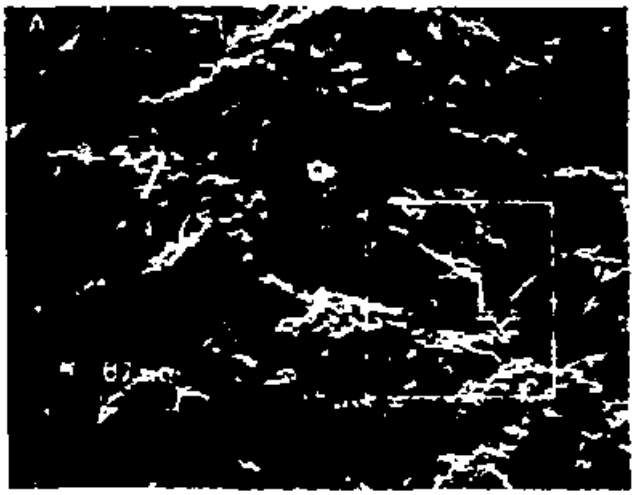

150X

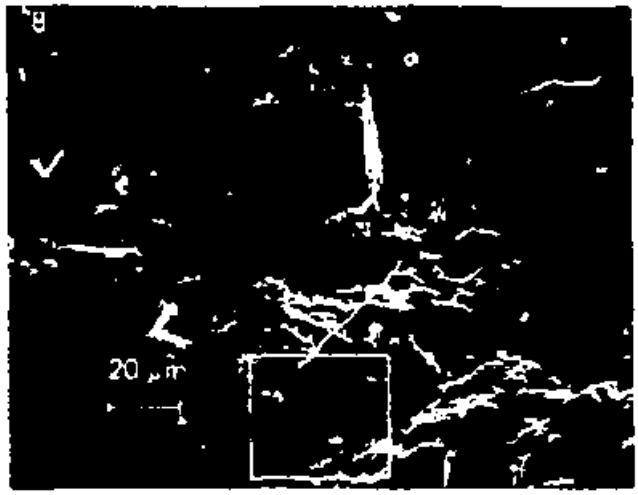

500X

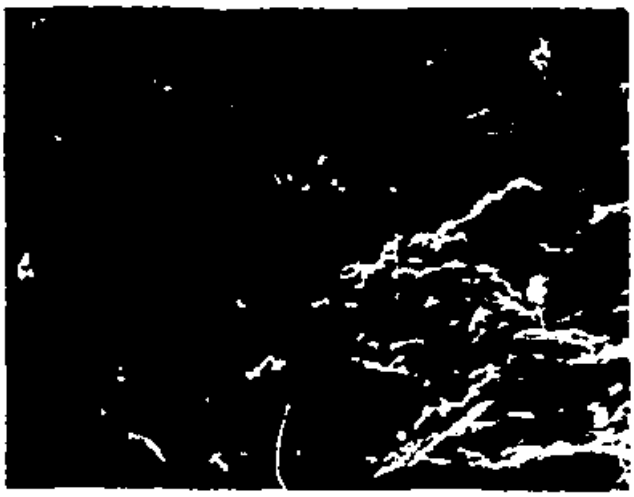

2500X

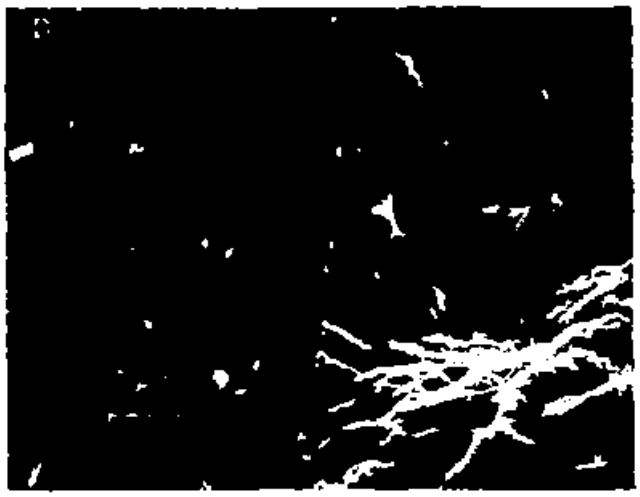

10 000X

Hoenig - Fig. 6

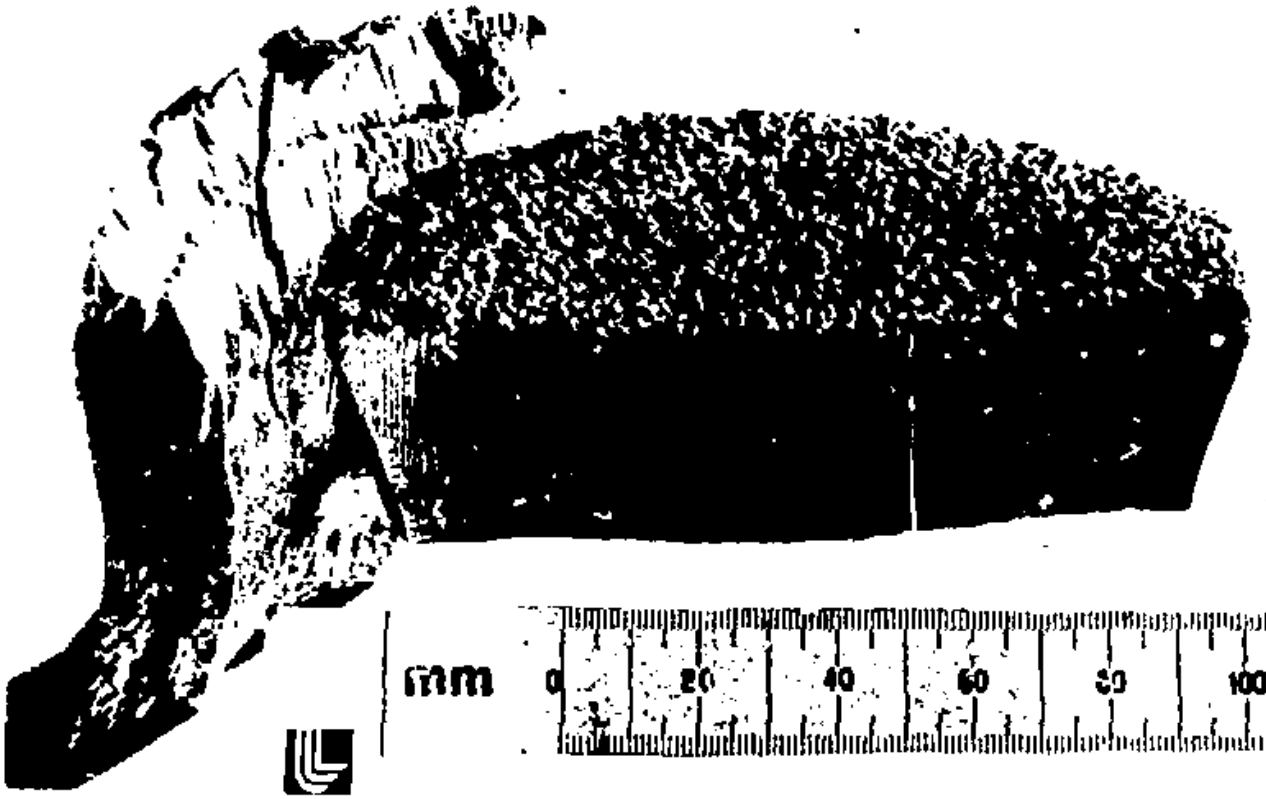

Hoenig – Fig. 7

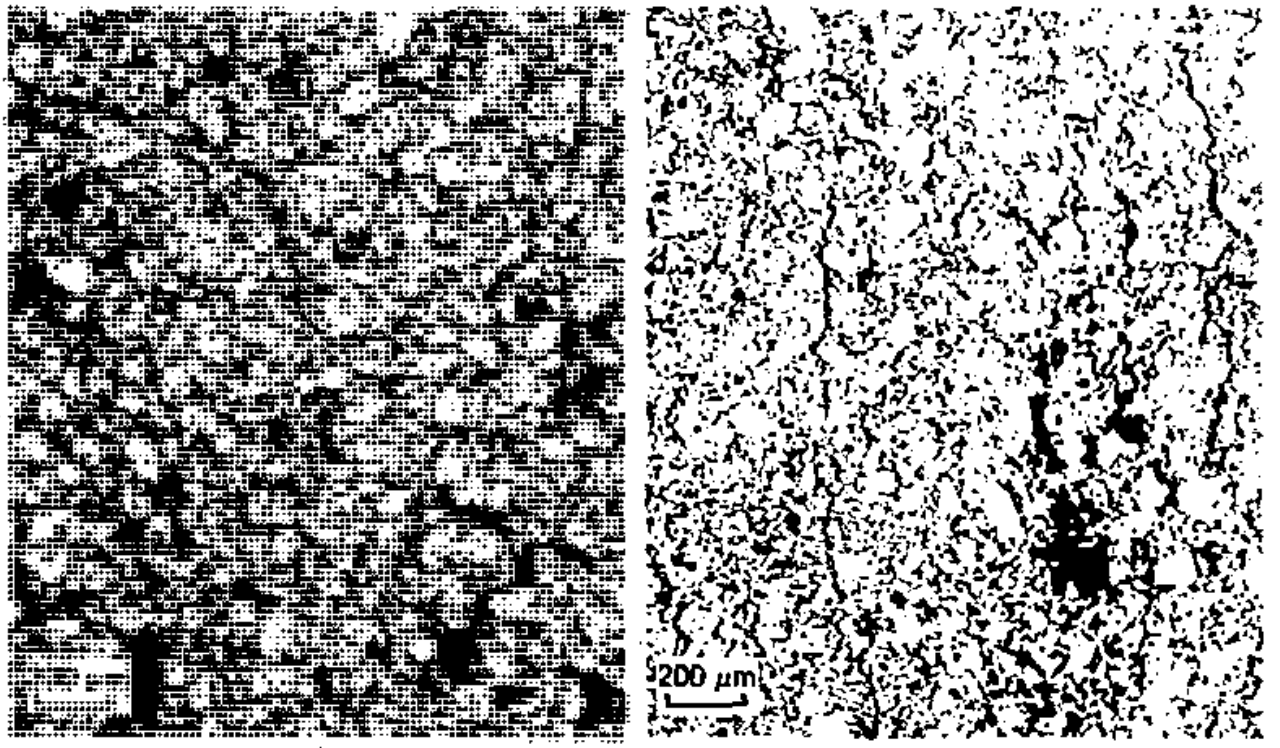

Hoenig - Fig. 8

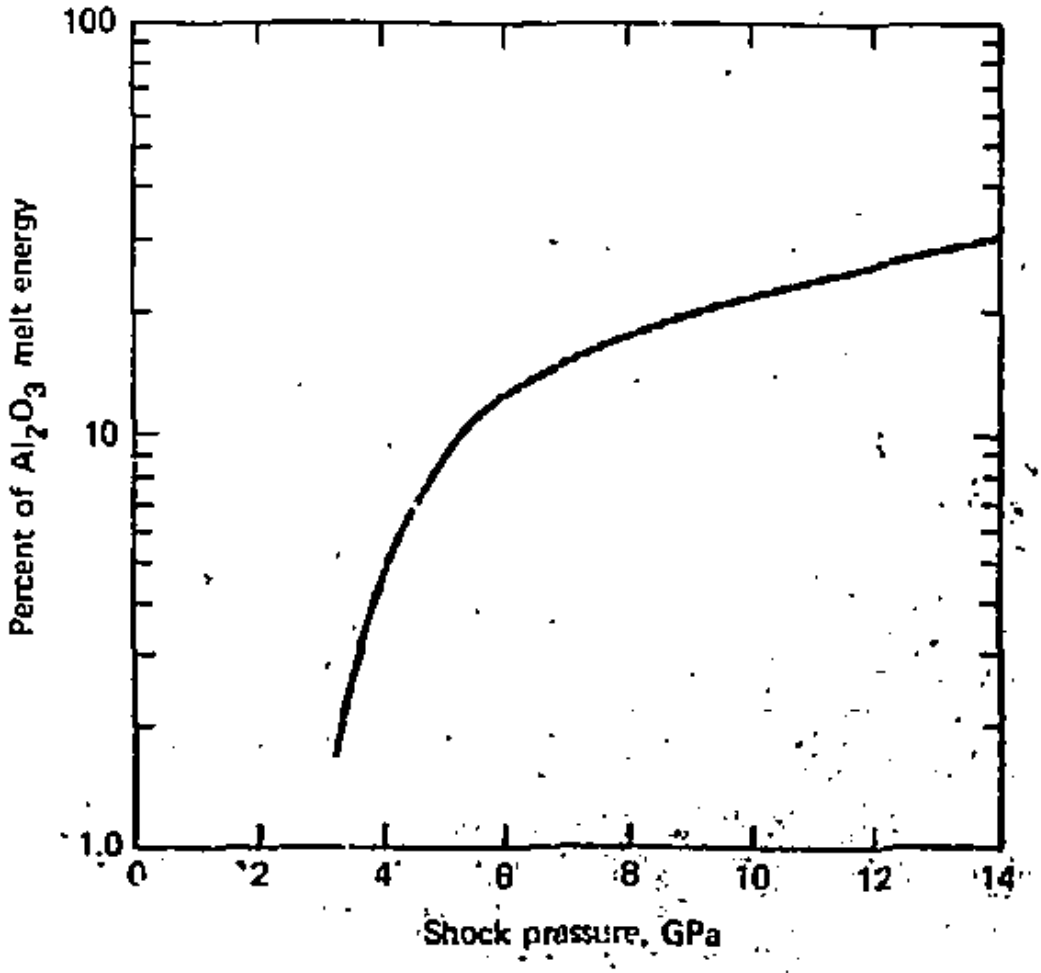
100
10
1.0
Percent of Al_2O_3 melt energy
0
2
4
6
8
10
12
14
Shock pressure, GPa

Hoenig – Fig. 9

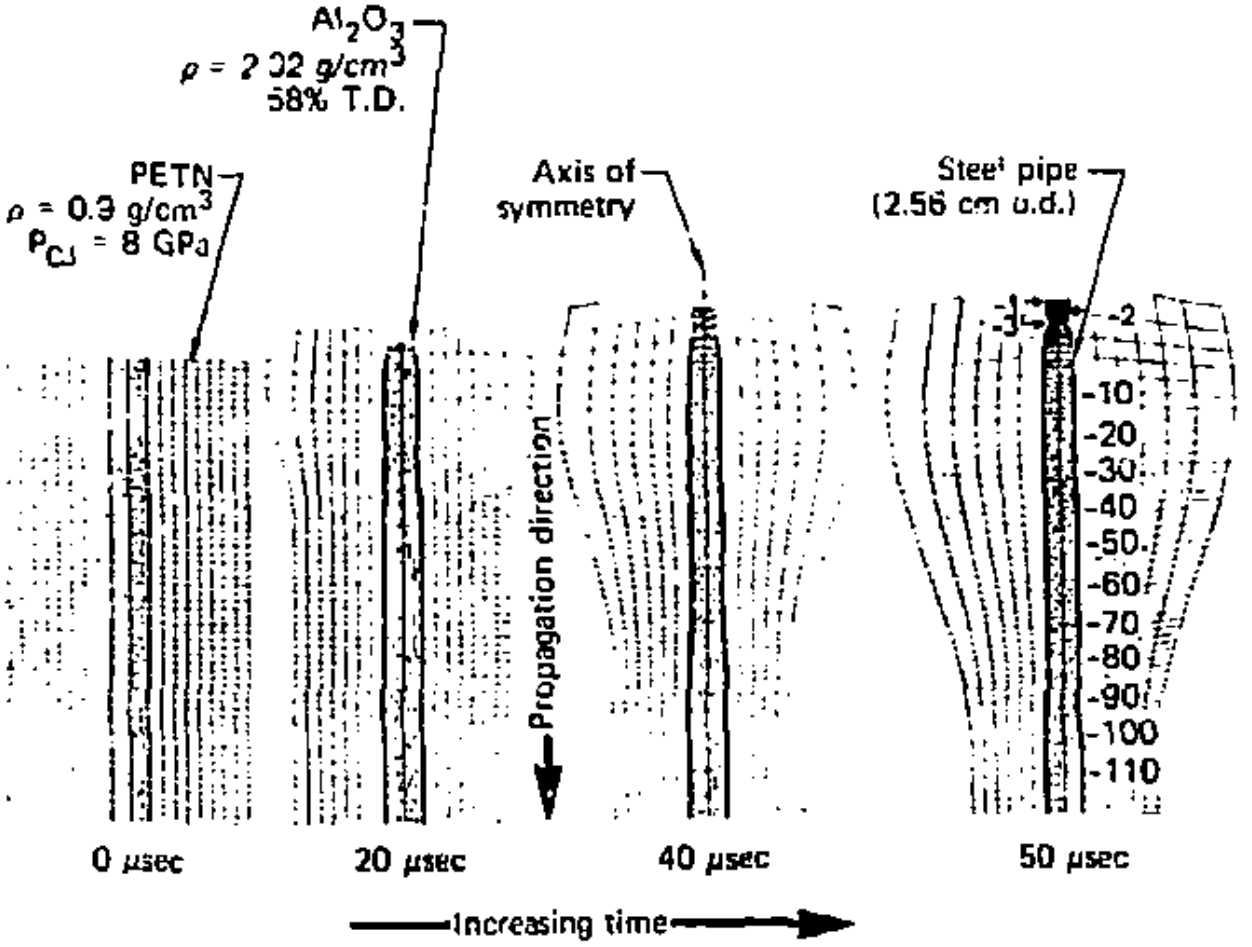

Boenig - Fig. 10

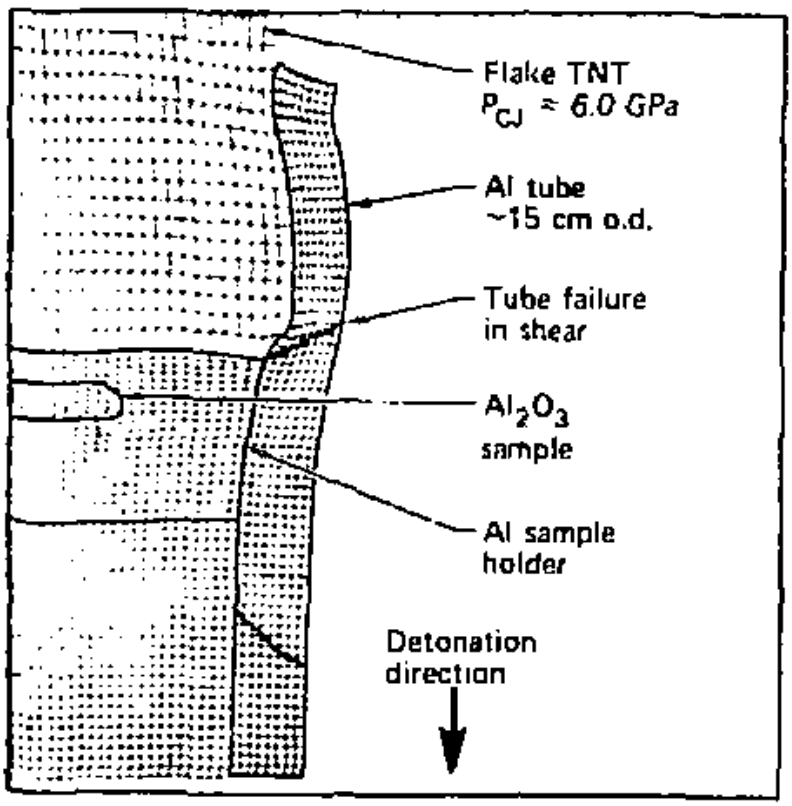

Hoenig - Fig. 11